Pharmaceutical Sciences and Drug Design
ISSN: 3062-4428
2026, Volume 6, Issue 1, Page No: 187-200

Available online at: www.galaxypub.co/page/journals

Galaxy Publication

Galaxy Publication

Dual-Targeted Aptamer/Transferrin-Functionalized Nanoparticles for Synergistic Delivery of Daunorubicin and Luteolin in Leukemia Therapy

Carlos Ramirez[1]*, Elena Torres[2], Pablo Ortega[1], Sofia Mendes[3]

[1]Department of Drug Discovery and Pharmaceutical Sciences, Faculty of Pharmacy, University of Barcelona, Barcelona, Spain.
[2]Department of Pharmaceutical Chemistry and Therapeutics, Faculty of Pharmacy, University of Lisbon, Lisbon, Portugal.
[3]Department of Drug Design and Innovation, Faculty of Pharmacy, University of Porto, Porto, Portugal.

* **E-mail** ✉ carlos.ramirez@gmail.com

Received: 02 February 2026; **Revised:** 06 April 2026; **Accepted:** 08 April 2026

ABSTRACT

The objective of this investigation was to construct a binary nanodrug-delivery system functionalized with aptamers (APs) and transferrin (Tf), and co-loaded with daunorubicin (Drn) and luteolin (Lut) for leukemia therapy. Ligand molecules bearing oligonucleotide AP and Tf were individually designed and fabricated. AP-functionalized Drn-loaded nanoparticles (AP-Drn NPs) along with Tf-Lut NPs were generated through a self-assembly process. An AP- and Tf-co-functionalized, Drn- and Lut-co-loaded nanodrug-delivery system (AP/Tf-Drn/Lut NPs) was subsequently produced by the self-assembly of AP-Drn NPs with Tf-Lut NPs. The in vitro and in vivo performance characteristics of this system were examined in a leukemia cell line and a tumor-bearing mouse model, and contrasted with single-ligand–functionalized, single-drug–loaded, and free-drug preparations. AP/Tf-Drn/Lut NPs possessed a spherical morphology and a nanoscale diameter (187.3 ± 5.3 nm), with roughly 85% drug-encapsulation efficiency. In vitro, the cytotoxic potency of AP/Tf-Drn/Lut NPs substantially exceeded that of single ligand–functionalized variants. Dual drug–loaded AP/Tf-Drn/Lut NPs demonstrated superior tumor-cell suppression compared with single–drug–loaded counterparts, reflecting a cooperative interaction between the two therapeutic agents. In vivo, AP/Tf-Drn/Lut NPs demonstrated the highest antileukemic efficacy with no detectable toxicity. The current investigation revealed that AP/Tf-Drn/Lut NPs represent a viable drug-delivery platform for the targeted management of leukemia, owing to the cooperative pharmacological interplay of the two agents within this construct. Constraints associated with this platform encompass stability issues during scaled-up manufacture and the translational pathway from preclinical research to clinical practice.

Keywords: Acute myeloid leukemia, Daunorubicin, Luteolin, Aptamer, Transferrin, Nanodrug-delivery system

How to Cite This Article: Ramirez C, Torres E, Ortega P, Mendes S. Dual-Targeted Aptamer/Transferrin-Functionalized Nanoparticles for Synergistic Delivery of Daunorubicin and Luteolin in Leukemia Therapy. Pharm Sci Drug Des. 2026;6(1):187-200. https://doi.org/10.51847/75ge0W92JY

Introduction

Acute myeloid leukemia (AML), a biologically heterogeneous hematologic cancer, constitutes the most frequently encountered acute leukemia in the adult population [1]. Treatment outcomes for individuals diagnosed with AML continue to be discouraging, with less than 30% attaining 5-year survival, alongside an elevated incidence and a mortality rate approaching 90% in elderly patients (> 65 years) [2, 3]. Existing therapeutic regimens for AML principally encompass conventional chemotherapy (a backbone of cytarabine combined with daunorubicin [Drn] or idarubicin), molecularly targeted intervention using FLT3 inhibitors like midostaurin, quizartinib, and cabozantinib, as well as immunotherapy, for instance gemtuzumab ozogamicin (an anti-CD33 monoclonal antibody linked to calicheamicin) [3-6]. Regrettably, contemporary treatments are still beset by therapeutic hurdles, such as diminished patient compliance arising from pronounced toxicity and restricted treatment

effectiveness rooted in drug resistance. Hence, the development of innovative therapeutic modalities to ameliorate treatment results is critically needed.

Nanoparticle (NP)-enabled combinatorial therapy has attracted considerable attention in recent years for the management of AML. At present, two liposome-based products are clinically accessible for HM therapy (liposomal Drn [DaunoXome] and liposomal cytarabine + Drn [CPX-351/VYXEOS]) [7, 8]. Phase III clinical data have exhibited that, compared to the administration of free pharmaceuticals (Drn and cytarabine), the liposomal formulation co-encapsulating Drn and cytarabine meaningfully prolongs median overall survival (9.56 vs 5.95 months) and elevates the overall remission rate (47.7% vs 33.3%) among older individuals with newly identified high-risk secondary AML [9]. This advancement heralds a transformative phase for AML sufferers built upon Drn-based combinatorial nanoformulation therapy.

As an anthracycline topoisomerase inhibitor, Drn is a broad-spectrum agent against hematologic malignancies, including AML, adult acute nonlymphocytic leukemia, and acute lymphocytic leukemia in both pediatric and adult populations [10]. However, the emergence of multidrug resistance has impeded the expanded clinical utilization of injectable Drn. In recent years, traditional Chinese herbal medicine and NPs have stimulated scholarly interest as means to circumvent multidrug resistance [11, 12]. Luteolin (Lut; 3′,4′,5,7-tetrahydroxyflavone) has a history of use in traditional Chinese medicine for addressing a spectrum of ailments, encompassing inflammatory conditions, cardiovascular disease, and cancer [13, 14]. A body of research has established that Lut can potentiate the antileukemic action of chemotherapeutic drugs and counteract multidrug resistance via mechanisms including P-gp and BCL2 upregulation, MCL1 downregulation, and the induction of apoptosis in HL60 cells, linked to c-Jun activation and histone H3 acetylation–dependent Fas/FasL expression [15-18]. A literature search failed to identify any reports of combinatorial leukemia treatment using Drn and Lut within a single nanoformulation. Consequently, the present study proposes that combination therapy with Drn and Lut may improve cytotoxicity and reduce multidrug resistance.

Aptamers (APs) bind their molecular targets with exceptional specificity and affinity, and AP-guided targeting platforms have been validated as promising for AML intervention [19]. Oligonucleotide APs can selectively associate with biomarkers on AML cells, among which the CD117 antigen is abundantly expressed [20]. Moreover, AML cells are known to overexpress a variety of cell-surface proteins, including transferrin (Tf) receptors. Targeted delivery of pharmaceuticals to neoplastic cells via the Tf receptor can be accomplished by attaching the Tf ligand onto the surface of NPs [21]. Polyethylene glycol (PEG) is a polymeric substance that can be employed as a tether for the covalent anchoring of assorted ligands. The terminal moiety of a PEG chain can be derivatized to present reactive amine, carboxylic acid, or sulfhydryl functionalities, permitting a diverse array of ligands to be efficiently coupled to the PEG chain covalently via amide linkages or disulfide-bridge construction [22]. In the present work, PEG served as a tether to realize both AP and Tf surface conjugation.

In this manuscript, an AP- and Tf-co-functionalized, Drn- and Lut-co-loaded binary nanodrug-delivery system (AP/Tf-Drn/Lut NPs) was engineered for AML-directed therapy. The in vitro and in vivo performance of this system was assessed in a leukemia cell line and a tumor-bearing mouse model, compared with single-ligand–functionalized, single-drug–loaded, and free-drug formulations.

Materials and Methods

Materials

Drn, Lut, oleic acid (OA), phosphatidylglycerol, iron-free human Tf, and N-hydroxysuccinimide (NHS) were procured from Sigma (St Louis, MO, USA). (2,3-dioleoyloxy-propyl)-trimethylammonium (DOTAP) was obtained through Avanti Polar Lipids (Birmingham, AL, USA). PEG-COOH (NH2-PEG-COOH), along with DSPE-PEG-COOH, was sourced from Ponsure Biological (Shanghai, China). The HL60 human leukocyte line was secured from the American Type Culture Collection (Manassas, VA) and propagated in Dulbecco’s modified Eagle’s medium (DMEM) enriched with 10% FBS under conditions of 37°C and a 5% CO2 atmosphere.

Animals

Female BALB/c nude mice, aged 4–6 weeks, were purchased from Beijing Vital River Laboratory Animal Technology (Beijing, China). All in vivo experimental procedures adhered to the National Institutes of Health Guide for the Care and Use of Laboratory Animals. The Animal Ethics Committee of Qingdao Hospital of Traditional Chinese Medicine approved the animal investigations.

Synthesis of AP–polyethylene glycol–oleic acid

The synthetic process commenced with the preparation of PEG-OA as outlined: NH2-PEG-COOH and TEA were dissolved in DMSO and subsequently transferred to a DMSO-based mixture containing OA, DCC, and NHS, followed by 12 h of stirring at ambient temperature [20]. The resultant OA-PEG-COOH underwent purification by filtration. In the next stage, a CD117-specific AP was linked to OA-PEG-COOH to construct AP-PEG-OA conjugates. Activation of OA-PEG-COOH was achieved with NHS, after which it was combined with a 5′-terminal amino-modified oligonucleotide CD117-specific AP possessing a functional amino group. The reaction was allowed to proceed with overnight mixing at room temperature, then purified by high-performance liquid chromatography (HPLC) and lyophilized. This yielded AP-PEG-OA conjugates as pale-white solids, and confirmation was performed using an enhanced BCA protein assay kit at 562 nm.

Synthesis of Tf-PEG-DSPE

The fabrication of Tf-PEG-DSPE involved establishing an amide bridge between Tf and DSPE-PEG-COOH [21]. A solution of DSPE-PEG-COOH, DCC, and NHS in DMSO was prepared and agitated for 10 h, after which Tf and TEA were added. The resulting mixture was stirred for an additional 10 h under a nitrogen atmosphere at room temperature, then filtered. Recovery of Tf-PEG-DSPE was accomplished through dialysis and lyophilization. Structural validation of Tf-PEG-PE was carried out by means of infrared spectroscopy and ^{1}H NMR.

Preparation of nanodrug-delivery system

AP-decorated Drn-loaded (AP-Drn) NPs **(Figure 1a)** together with Tf-Lut NPs **(Figure 1a)** were produced using a thin-film dispersion methodology [23]. Regarding AP-Drn NPs, a combination of AP-PEG-OA (200 mg) and Drn (100 mg) was dissolved in acetone (5 mL), and the solvent was then gently removed under reduced pressure using a hot-water bath (60°C) until a thin film formed. Subsequently, deionized water containing 0.5% (w/v) DOTAP was applied to the film, and AP-Drn NPs were generated via hydration. As for Tf-Lut NPs, Tf-PEG-DSPE (200 mg), Lut (100 mg), and phosphatidylglycerol (20 mg) were co-dissolved in acetone (5 mL), with the solvent then gradually evaporated under reduced pressure in a 60°C hot-water bath to afford a thin film. Deionized water was then introduced to hydrate the film, thereby yielding Tf-Lut NPs.

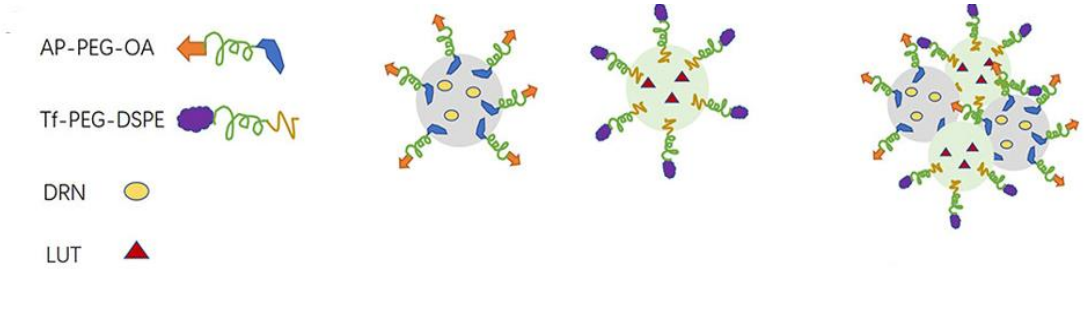

a)

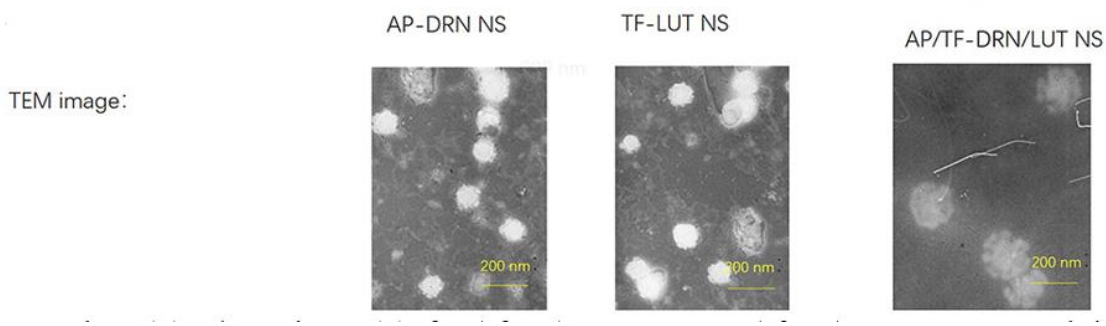

b)

Figure 1. Scheme (a) and TEM images (b) of AP/Tf-Drn/Lut NPs. Note: AP/Tf-Drn/Lut NPs were nanoscale in dimension and featured ligands distributed across the spherical surface.

The AP/Tf-Drn/Lut NP system **(Figure 1a)** was engineered through a self-assembly strategy [22]. AP-Drn NPs were introduced into the Tf-Lut NP dispersion with continuous agitation (400 rpm). For the preparation of the drug-free AP- and Tf-co-decorated binary nanocarrier (AP/Tf NPs), the same procedure was performed, omitting both drugs. Single AP- or Tf-decorated systems co-loaded with Drn and Lut (namely AP-Drn/Lut NPs or Tf-Drn/Lut NPs) were formulated by substituting PEG-OA for AP-PEG-OA or PEG-DSPE for Tf-PEG-DSPE, as appropriate. All finished NP formulations were lyophilized and kept at 4°C.

Characterization of nanodrug-delivery system

The morphological features of AP-Drn NPs, Tf-Lut NPs, and AP/Tf-Drn/Lut NPs were examined through negative staining employing a single droplet of a 3% aqueous sodium phosphotungstate solution, with subsequent visualization under transmission electron microscopy (JEOL, Tokyo, Japan) [24]. Particle sizing of the various nanodrug-delivery systems was conducted by dynamic light scattering (Beckman Coulter Delsa Nano C, Fullerton, CA). At the same time, ζ-potential values were recorded on a Zetasizer instrument (Malvern Instruments, Malvern, UK). Quantification of encapsulation efficiency (EE) and loading content (LC) for both Drn and Lut was carried out by HPLC fitted with a C18 column (150×4.6 mm, 12 nm), employing a mobile phase composed of 0.01 M KH2PO4, acetonitrile, and acetic acid in a volumetric ratio of 45:55:0.27, operated at a flow rate of 0.5 mL/min, with UV detection set at 350 nm for Lut and 490 nm for Drn, respectively [25, 26].

Stability of nanodrug-delivery system

The colloidal robustness of AP-Drn NPs, Tf-Lut NPs, and AP/Tf-Drn/Lut NPs was examined in both PBS and culture medium (DMEM supplemented with 10% FBS). Each nanosystem (20 mg) was dispersed into PBS or culture medium (10 mL) at pH = 7.4 and incubated at 37 °C for 4 days [27]. Fluctuations in particle size and EE were tracked using the identical measurement techniques referenced in the preceding sections.

In vitro release assays

The liberation kinetics of the encapsulated drugs from the nanocarriers were studied in vitro using a dialysis-based method with dialysis tubing having a 3500 Da molecular weight cutoff [28]. Aliquots (1 mL each) of AP/Tf-Drn/Lut NPs, AP-Drn/Lut NPs, Tf-Drn/Lut NPs, AP-Drn NPs, and Tf-Lut NPs were individually sealed inside dialysis bags and submerged in PBS (20 mL) containing 0.5% Tween 80, while being continuously agitated (100 rpm) at 37 °C. At designated time intervals, portions (200 μL) were collected from the release bath and promptly replaced with an equal volume of fresh buffer. HPLC subsequently analyzed the cumulative amounts of Drn and Lut released into the medium.

Cellular uptake

To gauge the degree of NP internalization by cells, the fluorescent probe coumarin 6 was co-incorporated with the therapeutic payloads, as described in the "Preparation of nanodrug-delivery system" subsection [29]. HL60 cells were seeded at 10^5 cells per well in a 24-well plate, exposed to the various nanodrug-delivery systems, and incubated for 1 and 24 h. Following incubation, the cells were rinsed three times with D-Hank's solution, harvested by centrifugation, and the cellular uptake was determined by flow cytometry using a BD FACSCalibur instrument.

Cytotoxicity assays

The antiproliferative activity of AP/Tf-Drn/Lut NPs and the comparator formulations was assessed through MTS assays [30]. HL60 cells were plated in a 96-well plate and left to settle overnight before the culture medium was replaced with fresh medium. The cells were subsequently treated for 48 h with AP/Tf-Drn/Lut NPs, AP-Drn/Lut NPs, Tf-Drn/Lut NPs, AP-Drn NPs, Tf-Lut NPs, free Drn/Lut in combination, free Drn alone, and free Lut alone. Following treatment, MTS solution (15 μL) was introduced into each well, and the plate was incubated for a further 4 h at 37 °C. Absorbance was measured on a microplate reader at 490 nm, and cell-survival fractions were calculated relative to untreated control wells, which served as the 100% viability baseline.

Drug combination

The nature of the pharmacological interaction between Drn and Lut was characterized using the combination index (CI) derived from the Chou–Talalay framework [31]. The CI at the 50% inhibition level (CI_{50}) was computed using the formula CI_{50} = (D)Drn/(D_{50})Drn + (D)Lut/(D_{50})Lut. In this expression, (D)Drn and (D)Lut refer to the individual concentrations of Drn and Lut present in the dual-drug construct (AP/Tf-Drn/Lut NPs) at the point of 50% cytotoxicity, whereas (D_{50})Drn and (D_{50})Lut correspond to the doses of every single drug administered via their respective single–drug–loaded nanosystems (AP-Drn NPs or Tf-Lut NPs) that elicit 50% cytotoxicity. Values of CI_{50} falling below 1 denote synergy, exactly 1 indicates additivity, and exceeding 1 signifies antagonism between the two agents.

In vivo AML-therapy efficiency

A subcutaneous leukemia-bearing mouse model was generated by injecting HL60 cells (10^6 cells in 150 μL PBS) into the left flank of BALB/c nude mice. Tumor dimensions were regularly monitored using caliper measurements, with tumor volume estimated by the formula: $L \times W^2/2$, where L is the longest tumor axis, and W is the widest axis perpendicular to L [32]. After tumor volumes reached approximately 100 mm^3, the mice were randomly assigned to 10 treatment cohorts (n = 8 per group). Intravenous injections were administered on days 0, 3, 6, 9, 12, 15, 18, and 21 with the following respective formulations: AP/Tf-Drn/Lut NPs (delivering Drn 5 mg/kg and Lut 2 mg/kg), AP-Drn/Lut NPs (Drn 5 mg/kg and Lut 2 mg/kg), Tf-Drn/Lut NPs (Drn 5 mg/kg and Lut 2 mg/kg), AP-Drn NPs (Drn 10 mg/kg), Tf-Lut NPs (Lut 4 mg/kg), AP/Tf NPs (empty dual-ligand nanocarrier), free Drn/Lut combination (Drn 5 mg/kg and Lut 2 mg/kg), free Drn (10 mg/kg), free Lut (4 mg/kg), and 0.9% saline as the vehicle control. Animal body weight was recorded throughout the 21-day experimental period. Additionally, blood chemistry markers — encompassing creatinine (Cre; reflecting renal function), alanine aminotransferase (ALT; reflecting hepatic function), and white blood cell (WBC) counts — were measured for safety evaluation.

In vivo pharmacokinetics and biodistribution

The mice were allocated at random into four cohorts (each containing eight animals) and given intravenous injections of AP/Tf-Drn/Lut NPs, AP-Drn/Lut NPs, Tf-Drn/Lut NPs, or the free Drn/Lut combination (all formulations provided Drn at 5 mg/kg and/or Lut at 2 mg/kg) [33]. Whole blood was sampled into heparinized receptacles at predefined intervals and centrifuged (1000 g, 10 min) to isolate the plasma fraction, which was then treated with a threefold excess of methanol and spun once again (1000 g, 5 min). Specimens of heart, liver, lung, kidney, spleen, bone marrow, and tumor mass were collected at 1 h and 48 h and homogenized in saline. Marrow from the femur and tibia was aspirated with RPMI medium (Gibco) supplemented with 5% FBS, using a 28-gauge needle [34]. Drug extraction from tissue homogenates was performed using a hexane–diethyl ether solvent mixture (3:1, v/v). The samples were centrifuged (1000 g, 10 min), and the upper organic phase was retained. The drug concentrations in both tissue and blood specimens were measured according to the protocol provided in the "Characterization of nanodrug-delivery system" subsection.

Statistical analysis

All outcomes are depicted as means ± SD. The statistical significance of observed differences was assessed using unpaired t-tests (for two groups) or one-way analysis of variance (for three or more groups), both conducted in SPSS 19.0. A threshold of $P < 0.05$ was adopted to denote statistical significance.

Results and Discussion

Characterization of AP-PEG-OA and Tf-PEG-DSPE

To verify conjugation of the AP to PEG-OA, the absorbance readings of the eluted fractions corresponding to AP-PEG-OA and to unbound AP were separately collected with an enhanced BCA protein assay kit at a wavelength of 562 nm. Free AP yielded a solitary peak with an elution window of 12 to 15 minutes, whilst AP-PEG-OA gave rise to two discrete peaks. The fact that one of these peaks matched the retention time of free AP confirmed that the AP moiety had been successfully tethered to PEG-OA. Structural authentication of Tf-PEG-DSPE was achieved through infrared (IR) spectroscopy and ^1H NMR. The IR spectrum featured signals at: 3621.3 (attributable to –NH– and –OH stretching), 1898.5 (–C=O), 1665.1 (–HN–CO–), and 1621.7 (–HN–CO–). ^1H NMR (recorded in $CDCl_3$, 300 MHz) displayed shifts δ (ppm) of: 0.89 ($–CH_3$), 1.12–1.97 (aliphatic DSPE

backbone protons), 2.33 (–$COCH_2$–), 2.42 (–$COCH_2CH_2$–), 2.61 (–CH_2N–), 3.39 (–OCH_3–), 3.70–4.10 (ethylene oxide protons of PEG), and 5.82 (–NH–). The isolated yields reached 73.9% for AP-PEG-OA and 78.6% for Tf-PEG-DSPE.

Characterization of nanodrug-delivery system

Electron micrographs revealed that AP/Tf-Drn/Lut NPs, AP-Drn NPs, and Tf-Lut NPs each assumed a globular architecture **(Figure 1b)**. AP/Tf-Drn/Lut NPs registered a mean diameter of 187.3 ± 5.3 nm **(Table 1)**, a measurement somewhat larger than that of AP-Drn NPs (91.5 ± 2.8 nm) and Tf-Lut NPs (88.7 ± 2.5 nm). With the sole exception of AP-Drn NPs, which exhibited a positive surface charge (18.9 ± 1.7 mV), every other formulation showed an electronegative ζ-potential. The EE across all preparations, including AP/Tf-Drn/Lut NPs, exceeded 85%. Over the complete 4-day evaluation period, particle size and EE of AP/Tf-Drn/Lut NPs, AP-Drn NPs, and Tf-Lut NPs remained essentially unchanged **(Figure 2a and 2b)**. This observation is consistent with earlier data published by Chen *et al*. [35] and supports the robust colloidal stability of these engineered nanosystems.

Table 1. Characterization of nanodrug-delivery systems (means ± SD, n=3).

Formulation	Lut LC (%)	Lut EE (%)	Drn LC (%)	Drn EE (%)	Zeta potential (mV)	PDI	Particle size (nm)
AP/Tf-Drn/Lut NPs	2.1 ± 0.4	85.9 ± 4.2	5.2 ± 0.5	88.7 ± 3.9	−25.4 ± 2.6	0.142 ± 0.019	187.3 ± 5.3
AP-Drn/Lut NPs	2.4 ± 0.6	86.7 ± 3.7	5.9 ± 0.6	87.5 ± 3.8	−19.2 ± 2.1	0.139 ± 0.023	186.7 ± 4.7
Tf-Drn/Lut NPs	2.2 ± 0.5	88.3 ± 3.9	5.7 ± 0.6	86.5 ± 4.1	−17.5 ± 1.8	0.126 ± 0.016	188.3 ± 4.5
AP-Drn NPs	—	—	11.8 ± 1.1	89.4 ± 4.4	+18.9 ± 1.7	0.112 ± 0.011	91.5 ± 2.8
Tf-Lut NPs	4.6 ± 0.7	86.5 ± 3.6	—	—	−38.9 ± 3.1	0.128 ± 0.014	88.7 ± 2.5
AP/Tf NPs	—	—	—	—	−37.6 ± 2.9	0.147 ± 0.026	187.8 ± 5.1

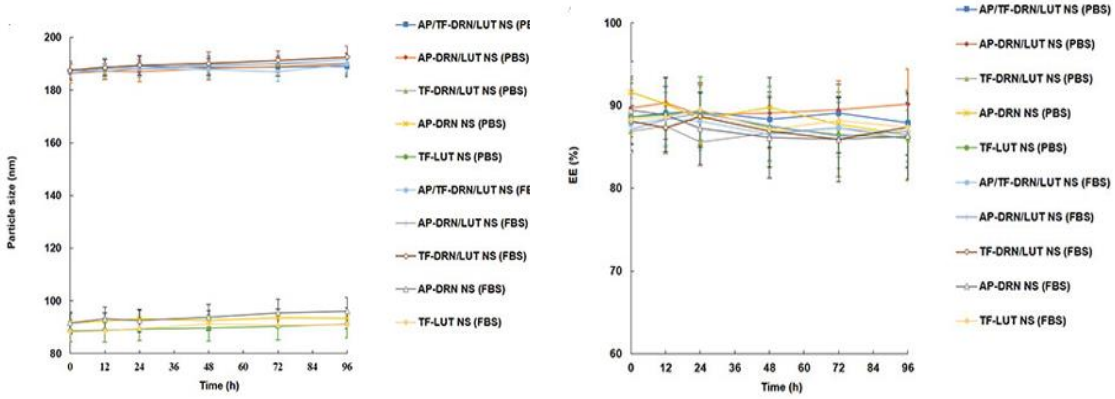

a) b)

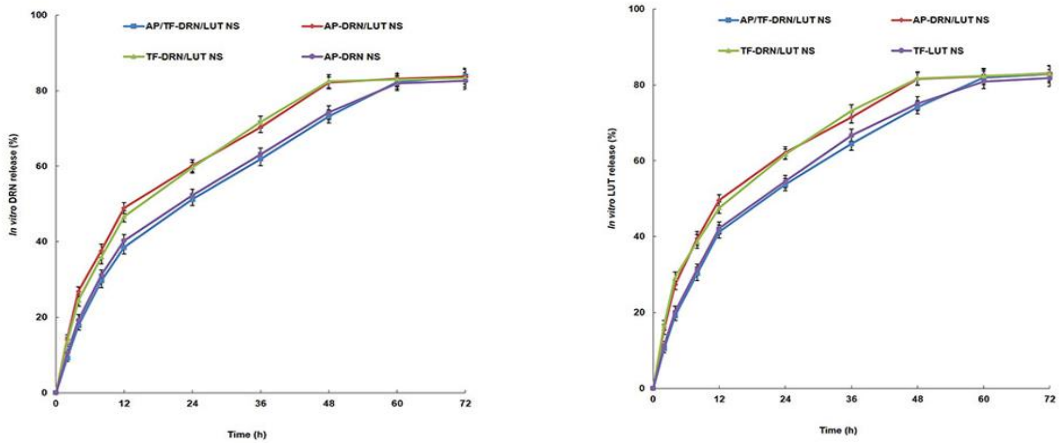

c) d)

Figure 2. Changes in particle size (a) and EE (b) were analyzed in PBS and culture medium (FBS). In vitro drug-release behavior of Drn (c) or Lut (d) from nanosystems evaluated by dialysis. Notes: Sustained drug-release patterns were found for all the samples tested. Data presented as means ± SD, n = 3.

In vitro release assays

A gradual, extended drug-release pattern was universally observed among all evaluated formulations **(Figure 2c and 2d).** The escape of both therapeutic agents from the dual-ligand-functionalized AP/Tf-Drn/Lut NPs was noticeably more retarded relative to the systems modified with only a single ligand (either AP or Tf). Considering the liberation of Drn as a representative case, it is evident from **Figure 2c** that AP/Tf-Drn/Lut NPs and AP-Drn NPs both required 60 h to discharge their Drn payload exhaustively. In contrast, AP-Drn/Lut NPs and Tf-Drn/Lut NPs reached the point of total release after just 48 h.

Cellular uptake

The extent to which the various nanosystems entered the cells is recorded in **Table 2**. All nanocarriers tested displayed pronounced internalization at both the 1 h and 24 h assessment points. The dual-ligand-modified AP/Tf-Drn/Lut NPs and the drug-free AP/Tf NPs exhibited uptake efficiencies that were clearly superior to those of their single-ligand-decorated equivalents ($P < 0.05$), lending credence to the cooperative targeting advantage afforded by employing the two ligands in tandem. This outcome echoes the findings previously described by Jing *et al.* [36].

Table 2. Cellular uptake percentages (means ± SD, n = 8).

Formulations	24 h	1 h
AP/Tf-Drn/Lut NPs	65.8 ± 3.3	73.1 ± 3.6
AP-Drn/Lut NPs	55.6 ± 2.8	59.5 ± 3.2
Tf-Drn/Lut NPs	54.2 ± 3.1	57.1 ± 2.9
AP-Drn NPs	53.1 ± 2.6	60.2 ± 3.3
Tf-Lut NPs	52.5 ± 2.8	58.4 ± 2.7
AP/Tf NPs	64.7 ± 3.2	74.3 ± 3.5

Cytotoxicity and drug combinations

When assessed for cytotoxic activity, AP/Tf-Drn/Lut NPs considerably outperformed both of the single ligand–decorated counterparts, namely AP-Drn/Lut NPs and Tf-Drn/Lut NPs ($P < 0.05$), **(Figure 3)**. Likewise, AP-Drn/Lut NPs and Tf-Drn/Lut NPs each elicited markedly stronger cytotoxicity than the free Drn/Lut combination ($P < 0.05$). The co-loaded AP/Tf-Drn/Lut NPs exerted greater tumor cell–suppressive effects than either of the individually loaded AP-Drn NPs or Tf-Lut NPs ($P < 0.05$), an outcome that points to a cooperative pharmacodynamic interplay between the two encapsulated agents. To lend quantitative support to this inference, CI_{50} values were derived and are collated in **Table 3**. Among the tested combinations, Drn and Lut co-formulated at a weight ratio of 5:2 produced the minimal CI_{50} value (0.792), signifying the strongest synergistic interaction. This 5:2 (w:w) Drn:Lut ratio was therefore adopted throughout the preparation of the delivery system.

Table 3. CI_{50} values of AP/Tf-Drn/Lut NPs when different Drn:Lut weight ratios were applied (means ± SD, n = 8).

Formulations	CI_{50}	IC_{50} of Lut (μM)	IC_{50} of Drn (μM)	Drn:Lut (w:w)
AP-Drn NPs	/	/	0.93 ± 0.09	/
Tf-Lut NPs	/	1.16 ± 0.12	/	/
AP/Tf-Drn/Lut NPs	0.987	1.06 ± 0.11	0.79 ± 0.08	5:1
AP/Tf-Drn/Lut NPs	0.792	0.22 ± 0.03	0.56 ± 0.05	5:2
AP/Tf-Drn/Lut NPs	0.872	0.45 ± 0.04	0.45 ± 0.04	1:1
AP/Tf-Drn/Lut NPs	0.941	0.73 ± 0.09	0.29 ± 0.03	2:5
AP/Tf-Drn/Lut NPs	0.969	0.90 ± 0.10	0.18 ± 0.02	1:5

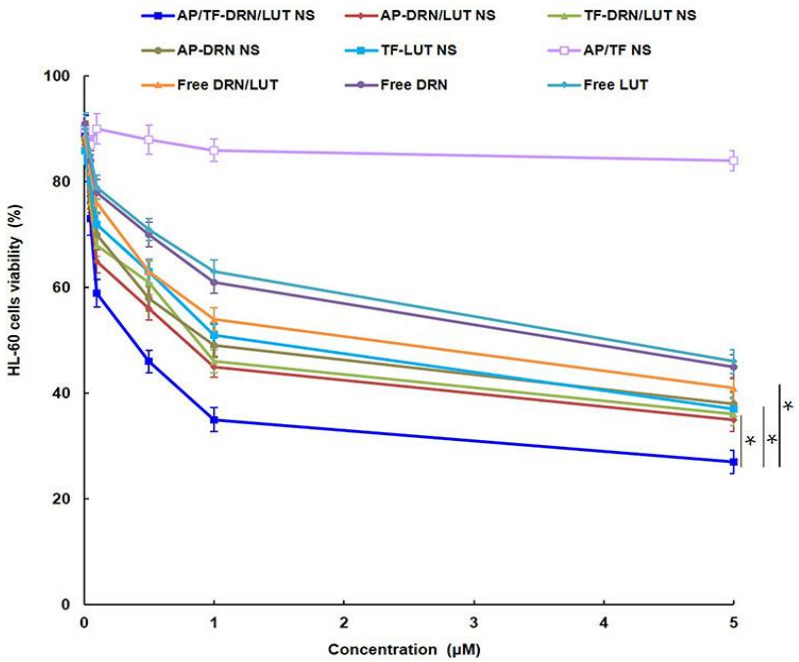

Figure 3. Cytotoxicity of AP/Tf-Drn/Lut NPs and other formulations evaluated with MTS assays. Notes: Cytotoxicity of AP/Tf-Drn/Lut NPs was remarkably higher than single ligand–decorated NPs, single drug–loaded NPs, and free drugs. Data presented as means ± SD, n = 6. $P < 0.05$.

In vivo AML-therapy efficiency

The data in **Figure 4a** show that all drug-inclusive formulations significantly reduced tumor growth compared with the saline-injected control arm ($P < 0.05$). The most pronounced antileukemic efficacy was achieved with AP/Tf-Drn/Lut NPs, surpassing those of single ligand–decorated, single drug–loaded, and free-drug regimens ($P < 0.05$). Across the board, drug-encapsulated nanosystems yielded superior AML-therapy outcomes compared with their free-drug counterparts ($P < 0.05$). Mouse body weights remained largely stable throughout the treatment period among groups receiving drug-loaded formulations, in stark contrast to the body weight losses recorded in both the saline control cohort and the cohort administered blank NPs ($P < 0.05$), **(Figure 4b)**. Animals treated with NP-based formulations exhibited near-baseline serum ALT and Cre levels, along with unaltered WBC counts, compared with the control group.

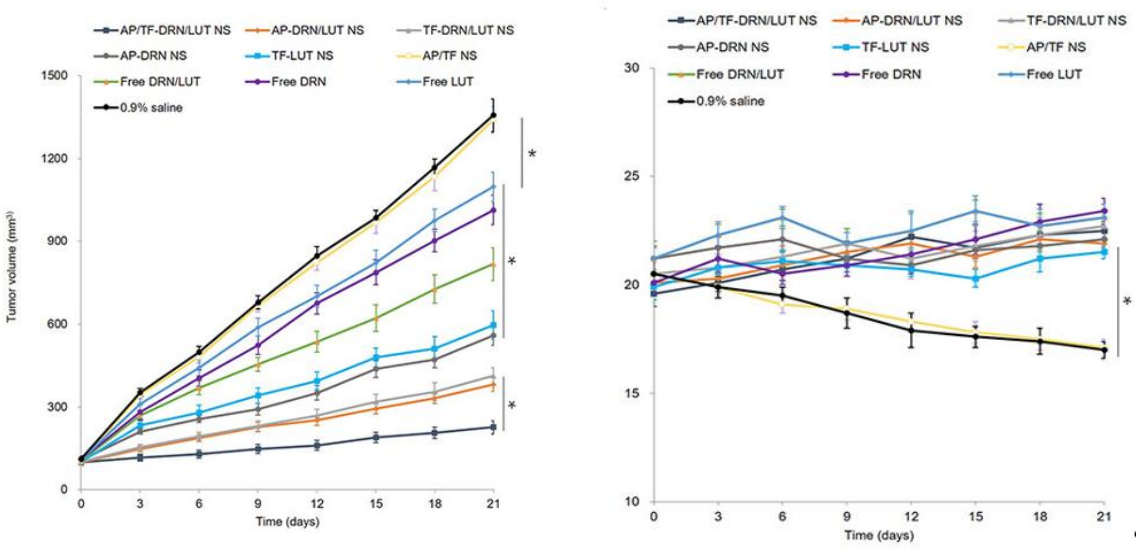

a) b)

Figure 4. In vivo AML therapy efficiency: Tumor size (a) and body weight (b). Notes: AP/Tf-Drn/Lut NPs exhibited the most remarkable AML therapy efficiency compared with single ligand–decorated, single drug–loaded, and free-drug groups. Data presented as means ± SD, n = 8. P < 0.05.

In vivo pharmacokinetics and biodistribution

The principal pharmacokinetic indices—encompassing area under the plasma concentration–time curve (AUC), peak plasma concentration (Cmax), and terminal elimination half-life (t½) — are detailed in **Tables 4 and 5**. Using the Lut-associated data as an illustrative case: the AUC determined for AP/Tf-Drn/Lut NPs (431.25 ± 11.38 mg/L/h) was significantly higher than those registered for AP-Drn/Lut NPs (311.26 ± 8.34 mg/L/h), Tf-Drn/Lut NPs (289.86 ± 7.65 mg/L/h), and the free Drn/Lut mixture (198.63 ± 4.59 mg/L/h; P < 0.05). Turning to Drn, both the Cmax (55.36 ± 3.21 L/kg/h) and t½ (12.37 ± 0.78 h) of AP/Tf-Drn/Lut NPs were substantially prolonged in comparison with the three alternative preparations. The organ- and tumor-specific biodistribution data are represented in **Figure 5**. At both the 1 h and 48 h post-injection intervals, AP/Tf-Drn/Lut NPs attained superior drug deposition within tumor tissue relative to the single ligand–decorated AP-Drn/Lut NPs and Tf-Drn/Lut NPs (P < 0.05); these latter systems, in turn, demonstrated significantly enhanced tumor localization when contrasted with free Drn/Lut (P < 0.05). In parallel, the free Drn/Lut formulation exhibited disproportionately greater accumulation in renal tissue at the 1 h time point compared with all drug-loaded nanosystems (P < 0.05).

Table 4. Pharmacokinetic parameters for Drn (means ± SD, n = 8)

Parameters	Unit	Free Drn/Lut	Tf-Drn/Lut NPs	AP-Drn/Lut NPs	AP/Tf-Drn/Lut NPs
C_{max}	L/kg/h	29.83 ± 2.88	40.55 ± 2.74*	42.31 ± 2.98*	55.36 ± 3.21*
$t_{½}$	h	1.89 ± 0.31	8.84 ± 0.53*	9.72 ± 0.64*	12.37 ± 0.78*
AUC_{0-t}	mg/L/h	256.81 ± 9.18	488.75 ± 21.16*	512.33 ± 17.14*	659.72 ± 19.56*
$AUC_{0-\infty}$	mg/L/h	404.73 ± 9.26	493.23 ± 22.44*	519.64 ± 19.47*	662.31 ± 20.05*

Note: P < 0.05 compared with free Drn/Lut. Abbreviations: Cmax = plasma drug peak concentration; t½ = half-life; AUC0–t = area under curve of time 0 to last time point; AUC0–∞ = area under curve of time 0 to maximum.

Table 5. Pharmacokinetic parameters for Lut (means ± SD, n=8)

Parameters	Unit	Free Drn/Lut	Tf-Drn/Lut NPs	AP-Drn/Lut NPs	AP/Tf-Drn/Lut NPs
C_{max}	L/kg/h	18.31 ± 2.12	26.59 ± 2.95*	28.11 ± 2.36*	35.47 ± 3.18*
$t_{½}$	h	1.51 ± 0.29	5.31 ± 0.34*	5.46 ± 0.41*	8.98 ± 0.58*
AUC_{0-t}	mg/L/h	198.63 ± 4.59	289.86 ± 7.65*	311.26 ± 8.34*	431.25 ± 11.38*
$AUC_{0-\infty}$	mg/L/h	202.34 ± 5.13	295.61 ± 6.96*	317.64 ± 11.35*	439.35 ± 12.24*

Note: P < 0.05 compared with free Drn/Lut. Abbreviations: Cmax = peak plasma drug concentration; t½ = half-life; AUC0–t = area under the curve of time 0 to last time point; AUC0–∞ = area under the curve of time 0 to maximum.

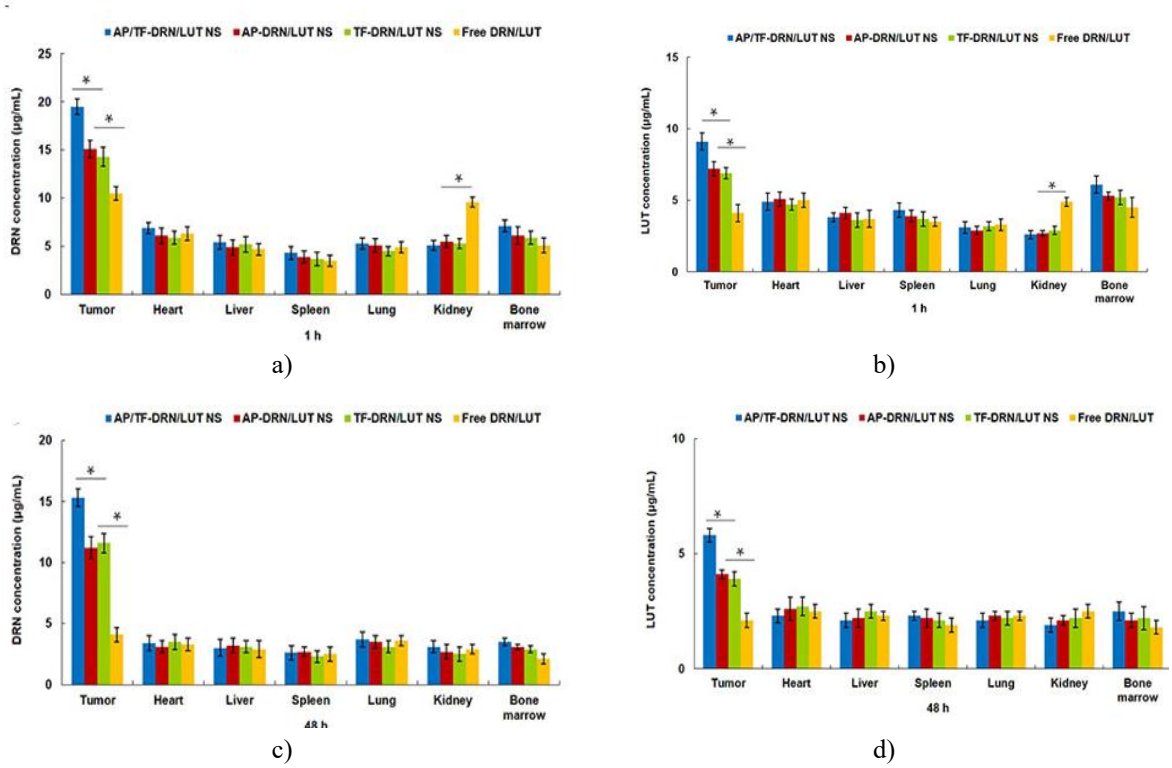

Figure 5. In vivo Drn (a and c) and Lut (b and d) distribution in tissue after 1 h (a and b) and 48 h (c and d) of drug administration. $P < 0.05$. Notes: AP/Tf-Drn/Lut NPs showed higher tumor-tissue distribution than single ligand–decorated AP-Drn/Lut NPs, Tf-Drn/Lut NPs, and free Drn/Lut. Data presented as means ± SD, $n = 8$. $P < 0.05$.

The primary intent of this research was to construct a binary nanodrug-delivery vehicle codecorated with AP and Tf and co-loaded with Drn and Lut for the treatment of AML. Initially, ligand constructs incorporating AP and Tf were separately devised and produced. Cationic AP-Drn NPs and anionic Tf-Lut NPs were independently generated, and subsequently AP/Tf-Drn/Lut NPs were assembled through electrostatic-driven self-assembly. Choueiri *et al*. [37] described how manipulating solvent composition or employing ligand electrooxidation can regulate polymer–solvent interactions. Their work broadens the spectrum of polymeric ligands suitable for NP assembly and patterning and paves the way for exploring previously uncharted self-assembly approaches. Yang *et al*. [38] devised pH/glutathione dual-responsive chitosan NPs via self-assembly/self-cross-linking, concluding that this strategy could overcome the drawbacks of conventional preparation methods, such as limited chemical stability, poor loading capacity, and photosensitizer release triggered by a single stimulus. Dong *et al*. [39] constructed dual-peptide ligand–modified NPs bearing hyaluronic acid and EGFR-targeting moieties, loaded with docetaxel and formononetin, to advance prostate cancer management. In the present investigation, AP/Tf-Drn/Lut NPs were specifically fashioned for leukemia treatment.

The particle size of AP/Tf-Drn/Lut NPs stood at 187 nm. Zhang *et al*. [40] reported that sub-200 nm dimensions can promote drug accumulation in tumor regions via the enhanced permeability and retention (EPR) effect, thereby enabling dose reduction and diminishing toxicity. The pattern of in vitro drug release is among the fundamental characteristics of NPs and carries considerable weight for pharmaceutical performance. Pang *et al*. [41] developed hyaluronic acid–functionalized NPs for simultaneous delivery of erlotinib and bevacizumab. Their work revealed that the release profiles of the two co-loaded drugs were similar, a result consistent with the experimental outcomes observed in the present study. In our work, the release of drugs from AP/Tf-Drn/Lut NPs proceeded more slowly than from systems bearing a single ligand (AP or Tf). This phenomenon can be interpreted as the denser ligand population on the NP surface retarding drug egress. Surface-anchored ligands can influence drug-release kinetics through steric obstruction, a conclusion also drawn by Dong *et al*. [39]. The incomplete attainment of 100% drug release may stem from the NP matrix physically entrapping a fraction of the payload, thereby impeding complete liberation.

Concerning in vitro cytotoxicity, AP/Tf-Drn/Lut NPs vastly outperformed the single ligand–decorated AP-Drn/Lut NPs and Tf-Drn/Lut NPs. The underlying explanation for this observation lies in the dual-ligand configuration, which bolsters the targeting precision of the NPs, amplifies intracellular drug levels, and thus yields superior therapeutic outcomes in cancer [42]. The dual drug–loaded AP/Tf-Drn/Lut NPs exerted greater tumor-cell suppression than their single–drug counterparts, AP-Drn NPs and Tf-Lut NPs, an improvement attributed to the synergistic pharmacodynamic interaction between the two therapeutic payloads. Li *et al*. [43] underscored that when combination regimens are employed in cancer chemotherapy, assessing the degree of synergy is of great importance, and CI analyses are among the most reliable approaches available. The Chou–Talalay framework was applied to classify the nature of the drug interaction as synergistic, additive, or antagonistic [44]. Among the tested proportions, the Drn:Lut weight ratio of 5:2 within the NPs produced the lowest CI_{50} value (0.46), indicating optimal synergistic interaction and was accordingly used to prepare the nanosystem.

Turning to the in vivo pharmacokinetics and biodistribution assessments, AP/Tf-Drn/Lut NPs exhibited favorable gains in AUC, Cmax, and t½, as well as tumor-tissue deposition. Moreover, the nanosystems exhibited prolonged circulation, a feature elaborated upon by Wang *et al*. [45]. In agreement with the present findings, Jedrzejczyk *et al*. [46] reported that a Tf-containing conjugate can serve as a delivery vehicle to elevate drug concentrations within leukemia cells that abundantly express surface Tf receptors, a result consistent with the tumor accumulation observed herein. The pronounced escalation in tumor-site accumulation afforded by drug-loaded nanosystems compared with simple drug solutions can be rationalized by the established concept that solid tumors possess inherently permeable microvasculature, allowing nanometer-scale particles to undergo passive tumor targeting through the enhanced permeability-and-retention mechanism [47]. Li *et al*. [48] further posited that reduced renal drug distribution can lower the incidence of adverse effects and improve antitumor performance. This profile was successfully realized by the nanosystems developed in this study.

Zhu *et al*. [49] reported that nanosystems can circumvent the toxicities associated with standard chemotherapeutic treatments while simultaneously achieving potent in vivo anticancer activity. Those authors deployed Tf-decorated NPs to amplify the AML-suppressive actions of drugs in a mouse model. He *et al*. [50] concluded that APs can engage cell-surface receptors and facilitate the cellular uptake of conjugated NPs, thereby serving as excellent targeting ligands within AP-guided drug-delivery platforms for oncological therapy. The current investigation established that AP/Tf-Drn/Lut NPs delivered the highest level of AML-therapy efficacy when benchmarked against single-ligand–decorated, single-drug–loaded, and free-drug formulations. This outcome aligned precisely with the study's core purpose—namely, the combined action of dual-targeting ligands and dual therapeutic agents. The body weights of mice receiving drug-carrying formulations exhibited no significant alterations, whereas animals in the saline control arm experienced a decline in body mass. Wang *et al*. [51] attributed this pattern to the likelihood that, over the course of treatment, mice may experience diminished food consumption, reduced energy levels, and decreased physical activity, collectively leading to weight loss. The AP/Tf-Drn/Lut NPs developed in this study demonstrated robust anticancer pharmacological efficacy, with near-total tumor-growth arrest and no toxicity, as evidenced by weight loss, results that align with those reported by Liu *et al*. [52].

Conclusion

In summation, AP/Tf-Drn/Lut NPs displayed strikingly elevated cytotoxicity relative to their single ligand–decorated counterparts. The dual drug–loaded AP/Tf-Drn/Lut NPs showed superior tumor-cell suppression compared with single–drug–loaded NPs, indicating synergistic pharmacodynamic interactions between the two encapsulated agents. AP/Tf-Drn/Lut NPs demonstrated the most potent antileukemic efficacy, with no in vivo toxicity, positioning them as a promising drug-delivery platform for targeted treatment of leukemia, a benefit derived from the cooperative action of the two drugs within this construct. The limitations inherent to this system encompass stability concerns during scaled-up manufacture and the translation of the application from bench to bedside.

Acknowledgments: None

Conflict of Interest: None

Financial Support: None

Ethics Statement: None

References

1. Estey E, Döhner H. Acute myeloid leukaemia. Lancet. 2006;368(9550):1894-907.
2. Daver N, Schlenk RF, Russell NH, Levis MJ. Targeting FLT3 mutations in AML: Review of current knowledge and evidence. Leukemia. 2019;33(2):299-312.
3. Huang X, Lin H, Huang F, et al. Targeting approaches of nanomedicines in acute myeloid leukemia. Dose Response. 2019;17(4):1559325819887048.
4. Ferrara F, Vitagliano O. Induction therapy in acute myeloid leukemia: Is it time to put aside standard 3 + 7? Hematol Oncol. 2019;37(5):558-63.
5. Lin M, Chen B. Advances in the drug therapies of acute myeloid leukemia (except acute promyelocytic leukemia). Drug Des Devel Ther. 2018;12:1009-17.
6. Norsworthy KJ, Ko CW, Lee JE, Pazdur R, Farrell AT, Justice R, et al. Mylotarg for treatment of patients with relapsed or refractory CD33-positive acute myeloid leukemia. Oncologist. 2018;23(9):1103-8.
7. Latagliata R, Breccia M, Fazi P, Carmosino I, Mancini M, Diverio D, et al. Liposomal daunorubicin versus standard daunorubicin: Long term follow-up of the GIMEMA GSI 103 AMLE randomized trial in patients older than 60 years with acute myelogenous leukaemia. Br J Haematol. 2008;143(5):681-9.
8. Maakaron JE, Mims AS. Daunorubicin-cytarabine liposome (CPX-351) in the management of newly diagnosed secondary AML: A new twist on an old cocktail. Best Pract Res Clin Haematol. 2019;32(2):127-33.
9. Lancet JE, Uy GL, Cortes JE, Newell LF, Lin TL, Ritchie EK, et al. CPX-351 (cytarabine and daunorubicin) liposome for injection versus conventional cytarabine plus daunorubicin in older patients with newly diagnosed secondary acute myeloid leukemia. J Clin Oncol. 2018;36(26):2684-92.
10. Kaspers GJ, Zimmermann M, Reinhardt D, Gibson BE, Tamminga RY, Aleinikova O, et al. Improved outcome in pediatric relapsed acute myeloid leukemia: Results of a randomized trial on liposomal daunorubicin by the international BFM study group. J Clin Oncol. 2013;31(5):599-607.
11. Jin J, Wang FP, Wei H, Liu G. Reversal of multidrug resistance of cancer through inhibition of P-glycoprotein by 5-bromotetrandrine. Cancer Chemother Pharmacol. 2005;55(2):179-88.
12. Hu CM, Zhang L. Nanoparticle-based combination therapy toward overcoming drug resistance in cancer. Biochem Pharmacol. 2012;83(8):1104-11.
13. Kim YS, Kim SH, Shin J, Harikishore A, Lim JK, Jung Y, et al. Luteolin suppresses cancer cell proliferation by targeting vaccinia-related kinase 1. PLoS One. 2014;9(10):e109655.
14. Chian S, Li YY, Wang XJ, Tang XW. Luteolin sensitizes two oxaliplatin-resistant colorectal cancer cell lines to chemotherapeutic drugs via inhibition of the Nrf2 pathway. Asian Pac J Cancer Prev. 2014;15(6):2911-6.
15. Zheng CH, Zhang M, Chen H, Li YX, Wang YJ, Zhao YL, et al. Luteolin from flos chrysanthemi and its derivatives: New small molecule Bcl-2 protein inhibitors. Bioorg Med Chem Lett. 2014;24(19):4672-7.
16. Danışman Kalındemirtaş F, Birman H, Candöken E, Bilgiş Gazioğlu S, Melikoğlu G, Kuruca S. Cytotoxic effects of some flavonoids and imatinib on the K562 chronic myeloid leukemia cell line: Data analysis using the combination index method. Balkan Med J. 2019;36(2):96-105.
17. Chen PY, Tien HJ, Chen SF, Chien MH, Hua KF, Cheng SP, et al. Response of myeloid leukemia cells to luteolin is modulated by differentially expressed pituitary tumor-transforming gene 1 (PTTG1) oncoprotein. Int J Mol Sci. 2018;19(4):1173.
18. Polier G, Giaisi M, Köhler R, Müller WW, Lutz C, Buss EC, et al. Targeting CDK9 by wogonin and related natural flavones potentiates the anti-cancer efficacy of the Bcl-2 family inhibitor ABT-263. Int J Cancer. 2015;136(3):688-98.
19. Wang M, Wu H, Duan M, Guo M, Wang Y, Li J, et al. SS30, a novel thioaptamer targeting CD123, inhibits the growth of acute myeloid leukemia cells. Life Sci. 2019;232:116663.
20. Zhao N, Pei SN, Qi J, Zeng Z, Iyer SP, Lin P, et al. Oligonucleotide aptamer-drug conjugates for targeted therapy of acute myeloid leukemia. Biomaterials. 2015;67:42-51.

21. Kim TH, Jo YG, Jiang HH, Lim SM, Youn YS, Lee S, et al. PEG-transferrin conjugated TRAIL (TNF-related apoptosis-inducing ligand) for therapeutic tumor targeting. J Control Release. 2012;162(2):422-8.
22. van Vlerken LE, Vyas TK, Amiji MM. Poly(ethylene glycol)-modified nanocarriers for tumor-targeted and intracellular delivery. Pharm Res. 2007;24(8):1405-14.
23. Nguyen CT, Tran TH, Amiji M, Lu X, Kasi RM. Redox-sensitive nanoparticles from amphiphilic cholesterol-based block copolymers for enhanced tumor intracellular release of doxorubicin. Nanomedicine. 2015;11(8):2071-82.
24. Mao K, Zhang W, Yu L, Yu Y, Liu H, Zhang X. Transferrin-decorated protein-lipid hybrid nanoparticle efficiently delivers cisplatin and docetaxel for targeted lung cancer treatment. Drug Des Devel Ther. 2021;15:3475-86.
25. El-Lakany SA, Elzoghby AO, Elgindy NA, Hamdy DA. HPLC methods for quantitation of exemestane-luteolin and exemestane-resveratrol mixtures in nanoformulations. J Chromatogr Sci. 2016;54(8):1282-9.
26. Yue Y, Eun JS, Lee MK, Seo SY. Synthesis and characterization of G5 PAMAM dendrimer containing daunorubicin for targeting cancer cells. Arch Pharm Res. 2012;35(2):343-9.
27. Wu R, Zhang Z, Wang B, Luo T, Song P, Deng Y, et al. Combination chemotherapy of lung cancer: Co-delivery of docetaxel prodrug and cisplatin using aptamer-decorated lipid-polymer hybrid nanoparticles. Drug Des Devel Ther. 2020;14:2249-61.
28. Wu C, Xu Q, Chen X, Liu J. Delivery luteolin with folacin-modified nanoparticle for glioma therapy. Int J Nanomedicine. 2019;14:7515-31.
29. Fan X, Wang T, Ji Z, Li Q, Shen H, Wang J. Synergistic combination therapy of lung cancer using lipid-layered cisplatin and oridonin co-encapsulated nanoparticles. Biomed Pharmacother. 2021;141:111830.
30. Haghighi FH, Binaymotlagh R, Mirahmadi-Zare SZ, Hadadzadeh H. Aptamer/magnetic nanoparticles decorated with fluorescent gold nanoclusters for selective detection and collection of human promyelocytic leukemia (HL-60) cells from a mixture. Nanotechnology. 2020;31(2):025605.
31. Chou TC. Drug combination studies and their synergy quantification using the Chou-Talalay method. Cancer Res. 2010;70(2):440-6.
32. Truebenbach I, Kern S, Loy DM, Schuster J, Schlosser S, Schmidt C, et al. Combination chemotherapy of L1210 tumors in mice with pretubulysin and methotrexate lipo-oligomer nanoparticles. Mol Pharm. 2019;16(6):2405-17.
33. Bao H, Zheng N, Li Z, Zhi Y. Synergistic effect of tangeretin and atorvastatin for colon cancer combination therapy: Targeted delivery of these dual drugs using RGD peptide decorated nanocarriers. Drug Des Devel Ther. 2020;14:3057-68.
34. Harris TJ, Green JJ, Fung PW, Langer R, Anderson DG, Bhatia SN. Tissue-specific gene delivery via nanoparticle coating. Biomaterials. 2010;31(5):998-1006.
35. Chen Y, Xu Z, Lu T, Luo J, Xue H. Prostate-specific membrane antigen targeted, glutathione-sensitive nanoparticles loaded with docetaxel and enzalutamide for the delivery to prostate cancer. Drug Deliv. 2022;29(1):2705-12.
36. Jing F, Li J, Liu D, Wang C, Sui Z. Dual ligands modified double targeted nano-system for liver targeted gene delivery. Pharm Biol. 2013;51(5):643-9.
37. Choueiri RM, Klinkova A, Pearce S, Manners I, Kumacheva E. Self-assembly and surface patterning of polyferrocenylsilane-functionalized gold nanoparticles. Macromol Rapid Commun. 2018;39(3).
38. Yang Z, Li P, Chen Y, Li Y, Wang H, Wang Y, et al. Construction of pH/glutathione responsive chitosan nanoparticles by a self-assembly/self-crosslinking method for photodynamic therapy. Int J Biol Macromol. 2021;167:46-58.
39. Dong Z, Wang Y, Guo J, Li Y, Lu X, Ma X, et al. Prostate cancer therapy using docetaxel and formononetin combination: Hyaluronic acid and epidermal growth factor receptor targeted peptide dual ligands modified binary nanoparticles to facilitate the in vivo anti-tumor activity. Drug Des Devel Ther. 2022;16:2683-93.
40. Zhang R, Ru Y, Gao Y, Li J, Mao S. Layer-by-layer nanoparticles co-loading gemcitabine and platinum (IV) prodrugs for synergistic combination therapy of lung cancer. Drug Des Devel Ther. 2017;11:2631-42.
41. Pang J, Xing H, Sun Y, Feng S, Wang S. Non-small cell lung cancer combination therapy: Hyaluronic acid modified, epidermal growth factor receptor targeted, pH-sensitive lipid-polymer hybrid nanoparticles for the delivery of erlotinib plus bevacizumab. Biomed Pharmacother. 2020;125:109861.

42. Wang H, Sun G, Zhang Z, Ou Y. Transcription activator, hyaluronic acid and tocopheryl succinate multi-functionalized novel lipid carriers encapsulating etoposide for lymphoma therapy. Biomed Pharmacother. 2017;91:241-50.
43. Li S, Wang L, Li N, Liu Y, Su H. Combination lung cancer chemotherapy: Design of a pH-sensitive transferrin-PEG-Hz-lipid conjugate for the co-delivery of docetaxel and baicalin. Biomed Pharmacother. 2017;95:548-55.
44. Chou TC. Theoretical basis, experimental design, and computerized simulation of synergism and antagonism in drug combination studies. Pharmacol Rev. 2006;58(3):621-81.
45. Wang B, Hu W, Yan H, Wang Y, Zhang C, Liu Y, et al. Lung cancer chemotherapy using nanoparticles: Enhanced target ability of redox-responsive and pH-sensitive cisplatin prodrug and paclitaxel. Biomed Pharmacother. 2021;136:111249.
46. Jedrzejczyk M, Wisniewska K, Kania KD, Marczak A, Szwed M. Transferrin-bound doxorubicin enhances apoptosis and DNA damage through the generation of pro-inflammatory responses in human leukemia cells. Int J Mol Sci. 2020;21(24):9390.
47. Choi J, Ko E, Chung HK, Kim D, Lee H, Kim IS, et al. Nanoparticulated docetaxel exerts enhanced anticancer efficacy and overcomes existing limitations of traditional drugs. Int J Nanomedicine. 2015;10:6121-32.
48. Li C, Ge X, Wang L. Construction and comparison of different nanocarriers for co-delivery of cisplatin and curcumin: A synergistic combination nanotherapy for cervical cancer. Biomed Pharmacother. 2017;86:628-36.
49. Zhu B, Zhang H, Yu L. Novel transferrin modified and doxorubicin loaded pluronic 85/lipid-polymeric nanoparticles for the treatment of leukemia: In vitro and in vivo therapeutic effect evaluation. Biomed Pharmacother. 2017;86:547-54.
50. He F, Wen N, Xiao D, Yan J, Xiong H, Cai S, et al. Aptamer-based targeted drug delivery systems: Current potential and challenges. Curr Med Chem. 2020;27(13):2189-219.
51. Wang L, Wang W, Rui Z, Zhou D. The effective combination therapy against human osteosarcoma: Doxorubicin plus curcumin co-encapsulated lipid-coated polymeric nanoparticulate drug delivery system. Drug Deliv. 2016;23(9):3200-8.
52. Liu B, Han L, Liu J, Han S, Chen Z, Jiang L. Co-delivery of paclitaxel and TOS-cisplatin via TAT-targeted solid lipid nanoparticles with synergistic antitumor activity against cervical cancer. Int J Nanomedicine. 2017;12:955-68.